Talanta 101 (2012) 307–313

Contents lists available at SciVerse ScienceDirect

Talanta

journal homepage: www.elsevier.com/locate/talanta

A preconcentrator chip employing μ-SPME array coated with in-situ-synthesized carbon adsorbent film for VOCs analysis

Ming-Yee Wong [a], Wei-Rui Cheng [b], Mao-Huang Liu [a], Wei-Cheng Tian [c], Chia-Jung Lu [b,*]

[a] Department of Chemistry, Fu-Jen Catholic University, New Taipei City, Taiwan
[b] Department of Chemistry, National Taiwan Normal University, 88, Section 4, Tingchou Road, Taipei 11677, Taiwan
[c] Department of Electrical Engineering, National Taiwan University, Taipei, Taiwan

ARTICLE INFO

Article history:
Received 12 June 2012
Received in revised form
14 September 2012
Accepted 17 September 2012
Available online 8 October 2012

Keywords:
VOCs
Preconcentrator
Micro-GC
SPME
Carbon adsorbent

ABSTRACT

We report the design, fabrication, and evaluation of a μ-preconcentrator chip that utilizes an array of solid-phase microextraction (SPME) needles coated with *in-situ*-grown carbon adsorbent film. The structure of the SPME needle (diameter=100 μm, height=250 μm) array inside the sampling chamber was fabricated using a deep reactive-ion etching (DRIE) process to enhance the attachable surface area for adsorbent film. Heaters and temperature sensors were fabricated onto the back of a μ-preconcentrator chip using lithography patterning and a metal lift-off process. The devices were sealed by anodic bonding and diced prior to the application of the adsorbent film. An adsorbent precursor, cellulose was dissolved in water and dynamically coated onto the SPME needle array. The coated cellulose film was converted into a porous carbon film via pyrolysis at 600 °C in a N_2 atmosphere. The surface area of the carbon adsorbent film was 308 m^2/g, which is higher than that of a commercial adsorbent Carbopack X. A preconcentration factor as high as 13,637-fold was demonstrated using toluene. Eleven volatile organic compounds (VOCs) of different volatilities and functional groups were sampled and analyzed by GC-FID, and the desorption peak widths at half height were all less than 2.6 s after elution from a 15 m capillary GC column. There was no sign of performance degradation after continuous operation for 50 cycles in air.

1. Introduction

Volatile organic compounds (VOCs) represent a class of contaminants that are hazardous to human health due to their diversity and toxicity. Although sophisticated analytical methods using a sorbent tube [1] or solid phase microextraction (SPME) [2–4] sampling followed by thermal desorption and gas chromatography–mass spectrometry (GC–MS) analysis have been well established and evaluated, the cost and time requirements for each GC–MS analysis often limits the use of such approaches for applications that need large quantities of continuous analysis data. Thus, the research on developing a rapid analysis instrument for VOCs remains an important issue in the field of analytical chemistry [5].

Many of the real-time or rapid analysis systems for VOCs rely on chemical sensors as their detection mechanism. In order to improve the detection limits, the most popular approach has involved the preconcentration of organic vapors onto adsorbents followed by thermal desorption to generate a high-concentration pulse. Early developments of micro-traps and preconcentrators were based on packing commercial adsorbents into glass or stainless steel capillaries and proved to be effective in enhancing the detection signal. Feng and Mitra [6] and Thammakhet et al. [7] demonstrated the use of a micro-trap as an online injector to enhance the signal for bench-top GC. Some earlier studies published by Zellers and co-workers established the design rule for a capillary preconcentrator and successfully combined it with a surface acoustic wave sensor array to produce micro-instruments for near-real-time VOC detection [8–11]. Many rapid detection systems have been explored using a capillary preconcentrator for sensitivity enhancement [12]. Additionally, planar-type preconcentrators using screen-printed carbon adsorbent film have also been examined [13,14]. The applications of systems built upon preconcentrators and sensor arrays include odor or halitosis sensing [15,16], explosive detection [17], breath analysis [10,18], and environmental VOCs such as chlorinated organics or aromatics [19–21].

In order to further improve the capability to analyze a complex environmental sample in near-real-time, the design of some miniature instruments had included a column separation mechanism and evolved into a micro-GC setup [22–24]. One of the most sophisticated designs reported by Zellers and Sacks incorporated a multistage preconcentrator, a tandem column

* Corresponding author. Tel.: +886 2 77346132; fax: +886 2 29324249.
E-mail address: cjlu@ntnu.edu.tw (C.-J. Lu).

0039-9140/$ - see front matter © 2012 Elsevier B.V. All rights reserved.
http://dx.doi.org/10.1016/j.talanta.2012.09.031

ensemble for tunable separation, and a sensor-array for pattern recognition. The analytical power to resolve mixtures of 30 compounds and quantify them at the ppb level has been demonstrated [25].

The first proven concept to use a micro electromechanical system (MEMS) to miniaturize GC was demonstrated early in 1979 by Terry et al. [26]. They fabricated an injection port, a wet-etched column and a thermal conductivity detector (TCD) on a 4" wafer. Some accessories such as gas cylinders, flow control units, and circuitries were still supported by off-chip lab facilities. Because of the advancements of MEMS technology in the past few decades, many novel MEMS components for GC, such as μ-detectors [27,28] and μ-columns [29–31], have been developed. The WIMS research center at the University of Michigan has recently completed a gas cylinder-free and fully functional "hybrid" μ-GC that integrates a MEMS-fabricated μ-detector, a μ-column, a μ-array detector, a μ-calibration source, and a μ-preconcentrator on a 4"-wafer [32].

As a part of the effort towards the ultimate miniaturization of μ-GC with high sensitivity, a μ-preconcentrator has become an important element as the front inlet for such a system. The key advantages of a MEMS μ-preconcentrator include a sharper desorption pulse, low energy consumption, and ease of integration with MEMS μ-GC [33,34]. The basic components of a μ-preconcentrator include a micro-fluidic channel that can be filled with adsorbent, and a micro-heater to achieve sample desorption. Some reports in the literature have discussed the internal flow distribution of μ-preconcentrators [35] and a design that can reduce heat capacity [36] for them. In order to facilitate the collection of volatile gases, commercial carbon adsorbents such as Carbopack X or Carboxene 1000 have normally been used to fill the fluidic channel [35–42]. There also have been studies that applied novel adsorbents such as carbon nano-powder [43] or carbon nanotubes [44] in μ-preconcentrators. Recently, an efficient process that uses ink-jet printing of dissolved polymer to create adsorbent films on MEMS μ-preconcentrators has been developed [45–48]. One of the advantages of forming such a conformal coating on micro-fabricated channels is that it provides better heat transduction between heaters and adsorbents, which could potentially reduce the time of desorption when less than few seconds of injection peak widths are required.

When considering the requirements of a higher surface area and durability at a high desorption temperature, porous carbon remains the most popular adsorbent for analytical application [49]. This work reports a new design that incorporates the idea of a SPME array to facilitate sampling efficiency. The carbon adsorbent coating on the MEMS–SPME array was directly grown on the surface via a pyrolysis process. Preconcentration factors and sampling capacity were investigated

2. Experimental

2.1. μ-Preconcentrator design and fabrication

The fluidic design on a silicon chip is shown in Fig. 1a. The width and depth of the inlet/outlet ports were both 250 μm, which allowed commercial deactivated capillary tubes, with specifications of 100 μm i.d./210 μm o.d., to be inserted with a reasonable margin. The end of the inlet port was tapped to a wider sampling chamber and filled with a needle array structure. Each needle was 100 μm in diameter with a height of 250 μm, which was later coated with adsorbent for SPME. Silicon needles were placed in an interlaced position so that airflow was forced to move in a turbulent manner to maximize the mass exchange of the gas flow. The height of the SPME needle and the depth of the

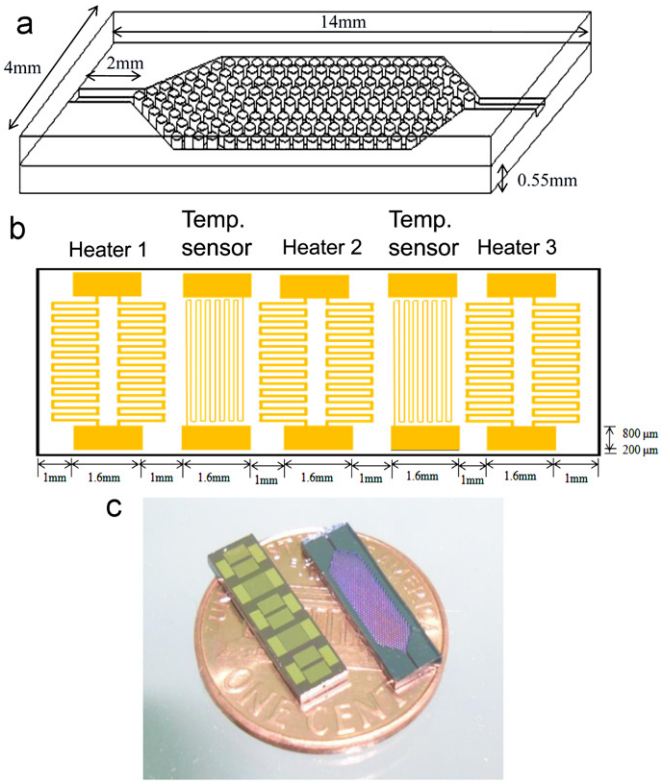

Fig. 1. Design diagram of device: (a) fluidic channel; (b) heater and temperature sensor and (c) device photo.

inlet/outlet channels were the same so that only one lithograph and one deep reactive-ion etching (DRIE) process were needed to complete the main fluidic structure. A glass wafer was anodic-bonded to the structure of the etched silicon wafer to provide the top seal of the fluidic chamber.

An oxidation layer was pre-deposited on the back surface of the silicon wafer to provide the insulation bases for heaters and temperature sensors. The heater and temperature sensors were fabricated on the backside of the silicon wafer using a standard lift-off process. Both heater and temperature sensors consisted of resistive wires based on patterned Au (3000 Å thick) film with Cr (50 Å thick) as an adhesive layer. Electric power was applied to resistive heaters to generate heat while the resistances of temperature sensor wires were read as a function of temperature. There were three heaters and two temperature sensors placed in an interchange order, as shown in Fig. 1b. Each heater consisted of two parallel (50 μm in width) and short (2.8 cm in length) gold wires to allow for a follow-through current with an overall resistance of 80 Ω for each heater. The temperature sensors were 10 μm wide and 8.2 cm long Au wires set in a serpentine shape with a temperature sensor resistance of 1.6 kΩ. The film thickness of the heaters and temperature sensors were the same in order to simplify the fabrication process to one lithograph and one metal lift-off only. The wafer was diced after the fabrication of the μ-channel and temperature control elements. The dimensions of each device were $4 \times 14\ mm^2$. The fine structure inside the fluidic chamber was inspected using a scanning electron microscope (ERA-8800FE, ELIONIX, Japan).

2.2. Carbon adsorbent film synthesis

Cellulose was obtained from Aldrich (Milwaukee, WI, USA) and dissolved in deionized water in a 10% (w/v) concentration. Gentle heating and stirring were needed during the dissolution process.

When the solution was cooled to room temperature, the viscosity increased. The cellulose solution was drawn through the fluidic channel using a peristaltic pump (MasterFlex 7518-10, Cole-Parmer). After the channel was filled with a cellulose solution, the inlet tube was removed from the solution and air was drawn through the channel to leave a thin viscous coating on the wall of the μ-channel and silicon needles. After this coating step, the connection tubes for coating liquid were removed and the chip was placed in a tube oven with a continuous flow of N_2. The oven temperature was raised to 100 °C for 1 h for an initial drying of the coating film. The oven temperature was then ramped up at the rate of 20 °C/min to 600 °C where it was held for 2 h. The oven was then powered off to allow cooling to room temperature while N_2 was continuously flowed through to maintain an oxygen-free atmosphere. The chip was removed from the oven after cooling to room temperature. The black color of carbon film could be seen inside the sampling chamber (refer Appendix). The mass of adsorbent film was determined to be approximately 2 mg by weighing the μ-preconcentrator chip before and after the implantation of the adsorbent film. The BET surface area of the pyro-synthesized carbon film was measured using a Physisorption analyzer (ASAP2010, Micromeritics, USA).

2.3. Device packaging and connection

After the completion of the carbon film formation, two deactivated silica capillary tubes (100 μm i.d., Supelco, Bellefonte, PA, USA) were inserted into the inlet and outlet ports of the μ-preconcentrator. A polyimide sealing resin (Supelco), that could sustain temperatures as high as 350 °C was applied and cured at 150 °C to provide a gas-tight seal between the capillary tube and the port channel wall. A square hole of the same size and shape as the μ-preconcentrator chip was drilled at the center of a printed circuit board (Fig. 2a) leaving only two small contact bridges at both ends. The small area of these contact bridges minimized the heat lost from the μ-preconcentrator to the circuit board. The μ-preconcentrator chip was positioned in the center hole of the circuit board with the glass side glued down to the contact bridges using the same polyimide resin mentioned above. The temperature of the contact bridges was expected to be much lower than that of the μ-preconcentrator chip during thermal desorption due to the low thermal conductivity of glass. The inlet and outlet capillary tubes were fixed on the circuit board using regular A/B epoxy to prevent the tube bending during later experiments (Fig. 2b).

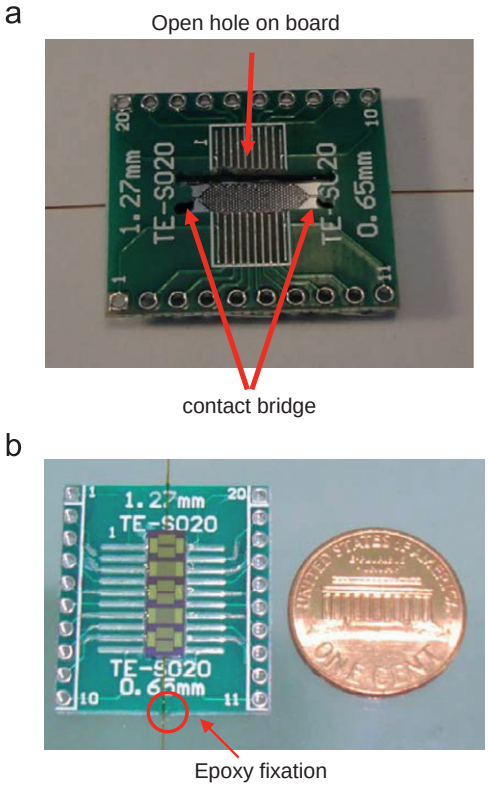

Fig. 2. (a) Front picture of the device on a circuit board and (b) photo after completion of packaging.

The heaters and the sensors were wire-bonded to the contact pad of the printed circuit board for further connections to a power supplier and to resistance measurement circuitry. Each electrical connection of the μ-preconcentrator chip was multi-bonded with aluminum wire to reduce the current loading of each wire and to prolong the device's working lifespan in case of the failure of one or two wire connections. A picture revealing the details of the wire bond is shown in the Appendix. The temperature of the μ-preconcentrator chip during the heater and temperature sensor operation was confirmed via thermal images measured by infrared camera (FLIR A325, FLIR systems, USA).

2.4. Breakthrough test

Standards of VOCs in the ppb range were prepared via two-stage dilutions in Tedlar bags. The first stage was generated by injecting a small aliquot of pure organic liquid with gentle heating followed by cooling to room temperature. This first stage concentration was in the range of hundreds of ppm, which is much lower than the saturated vapor concentration at room temperature to ensure complete evaporation. A small portion (1–10 mL) of the first stage sample was transferred to another Tedlar bag filled with clean air (1–3 L). The dilution factor was several hundreds to thousands, and the final concentration was calculated to be in the ppb range.

Fig. 3 shows the configuration of the preconcentration test system. The heart of this test system was a 6-port valve (E2C6UWT-110, VICI. Valco Instruments, USA) that is commonly used for sample injection in chromatographic experiments. When the valve was in the "load" position, ppb-level vapors in a Tedlar bag were drawn through the μ-preconcentrator via a diaphragm pump (N86KNDC, KNF Neuberger, Germany). The sampling flow rate was adjustable through a downstream needle valve. Different lengths of sampling time (e.g. 1.0–35 min) were tested and sampling volumes were calculated accordingly. After the designated sample volume had been reached, the electrical power for heaters was turned on via a computer-controlled solid-state relay. All three heaters on the μ-preconcentrator chip were connected in parallel to the same relay. The resistance changes of the temperature sensor were converted to voltage changes via a Weston bridge circuit and were measured via a personal computer through an analog-to-digital interface (USB-6211, National Instruments, USA) and a LabVIEW program written in-house. The heater power was automatically switched on and off by using the temperature reading feedback to control the desorption temperature at a preset value. After the desorption temperature was reached, the 6-port valve was switched to the "inject" position, and carrier gas was flushed through the μ-preconcentrator. The heating time of a μ-preconcentrator is only a few seconds. The commercial thermal desorption system uses liquid nitrogen focusing, therefore it can slowly heat up the adsorbent tube while carrier gas is flushing through. As for a μ-preconcentrator, the desorption temperature must be reached prior to carrier flush so that minimum peak width can be obtained without liquid nitrogen focusing. The thermally desorbed sample was carried into the

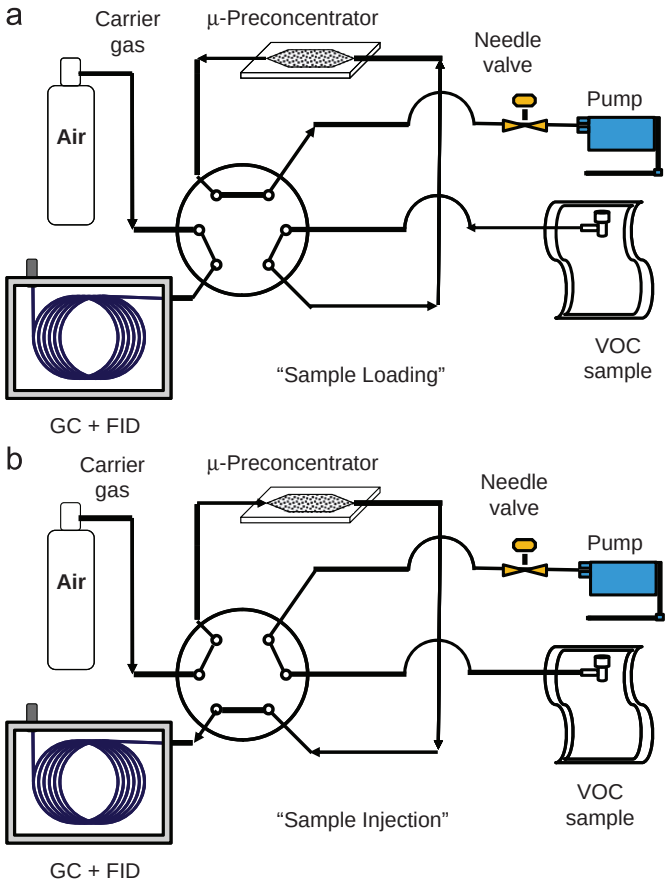

Fig. 3. Breakthrough test setup: (a) sample loading and (b) sample injection.

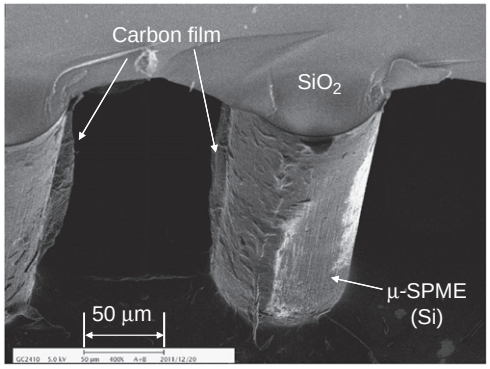

Fig. 4. Cross section SEM images of μ-SPME array coated with carbon film.

capillary column (DB-5, 0.32 mm i.d., 15 m long, Supelco) to be detected by an Agilent 5890 GC-FID.

3. Results and discussion

3.1. Device and carbon film structure

The μ-preconcentrator chip was scratched and cracked open to reveal the interior structure. Fig. 4 shows the interior SEM image of a carbon adsorbent film coated device. The adsorbent film was tightly attached to the structure of silicon needles. The film thicknesses were not perfectly uniform on the needles. The thickest part of the carbon film was approximately 10 μm, as measured from the SEM image. The total mass of carbon

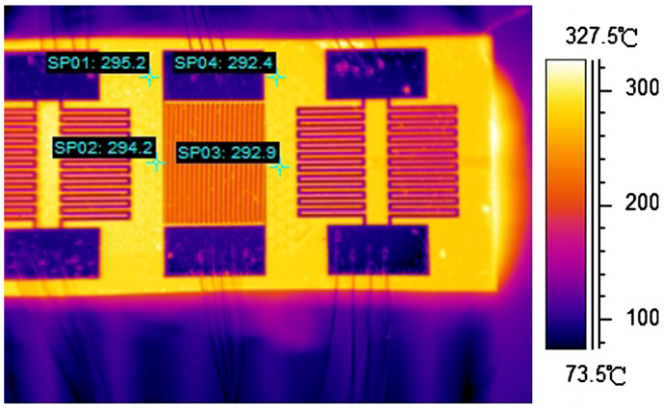

Fig. 5. Infrared image and temperature measurement of μ-preconcentrator after heater power turns on.

adsorbent film inside the μ-preconcentrator was approximately 2 mg, as measured by the weight difference before and after the deposition of carbon film. The BET surface area measured using N_2 adsorption at 77 K was 308 m^2/g. This value is significantly higher than a commercial adsorbent Carbopack X (250 m^2/g). Other than cellulose, we did try to use other carbohydrates such as fructose, glucose or polymers such as polyethylene glycol as the precursor for producing carbon film. None of the carbon films from other precursors showed the appreciable preconcentration behavior as cellulose-generated carbon film.

3.2. Performance of μ-heater

Fig. 5 shows the infrared image of the backside of a μ-preconcentrator when the heater power was applied to maintain a temperature near 300 °C. This image shows the right half of the chip, which includes two pairs of heaters and a temperature sensor. The corresponding color scale for temperature is shown on the right of this figure. Four specific points of temperature measurement around the temperature sensor are labeled. The temperature values ranged between 292.4 °C and 295.2 °C. Although silicon is a high-thermal conductive material, a few degrees of temperature gradient remained across the chip. The cooler region at the rear of the μ-preconcentrator, which is located outside the right heater in Fig. 5 was the region of the tube connection and no adsorbent was to be heated on the other side. Since the highest sustainable temperature for polyimide sealing resin on the outside of connecting capillary tubes is 350 °C, we might be able to raise the center temperature to as high as 360 °C for a short period of time without severe damage to the gas-tight seal.

3.3. Optimizing desorption temperature

In order to determine the suitable desorption temperature, we picked toluene as the representative compound for desorption tests. The same amount of toluene (100 ppb, 50 mL) samples were collected using a μ-preconcentrator with desorption at various temperatures. Fig. 6 shows a collection of desorption peaks at different desorption temperatures ranging from 360 to 240 °C. The desorption peak heights were identical from 360 to 320 °C. The peak area began to reduce when desorbed at temperatures of 300 °C or lower, which could be a sign of incomplete desorption. The desorption efficiency was calculated by dividing each desorption peak area to the maximum peak area at high desorption temperature. The desorption efficiency in the temperature range between 320 °C and 360 °C was 100%. Desorption efficiencies for lower temperatures

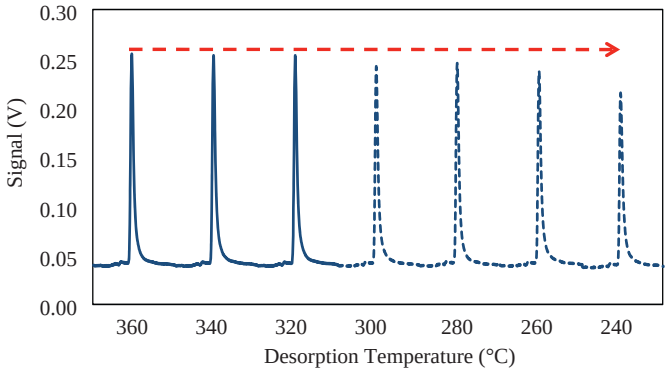

Fig. 6. Desorption peaks at various temperatures.

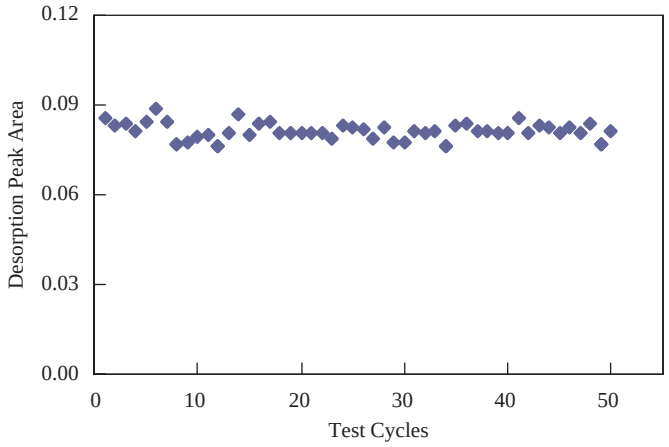

Fig. 7. Desorption peak areas of 50 replicates using air as the carrier gas.

were: 300 °C (96%), 280 °C (93%), 260 °C (91%) and 240 °C (89%). In the interest of prolonging the device lifetime, the lowest desorption temperature that would not reduce the peak area, 320 °C, was chosen for all later experiments. The residual tests with a second heating at 320 °C were also performed to confirm that no measurable peak was found in the second desorption. The power consumption for reaching and maintaining 320 °C was 3.6 W which was calculated from a driving voltage of 16.5 V and a flow-through current of 0.217 A.

3.4. Reproducibility of the μ-preconcentrator

Fig. 7 shows the peak areas of 50 consecutive sample-and-desorption cycles for toluene using a μ-preconcentrator. In order to complete all samples in one Tedlar bag containing 200 ppb toluene, we sampled at 40 mL/min for 1 min only. The total sample volume for all 50 runs was 2 L. There was no consistent decay tendency in peak areas beyond the 50 runs. Desorption peak areas did vary randomly around the mean from shot to shot. The coefficient of variation (C.V.) was equal to 3.3%. This 3.3% variation was the sum of instabilities in the sampling pump, the μ-preconcentrator, and the GC-FID. The variation in sampling time also contributed to the overall variations since we only sampled for 1 min. This result shows that the μ-heater can repeatedly heat to 320 °C and be cooled to room temperature for 50 times without degradation. The gas-tight seal provided by the polyimide resin sustained the same temperature cycles without leakage.

3.5. Preconcentration factor

The preconcentration factor was calculated using the peak area ratio between the preconcentrated peak and the non-preconcentrated peak. We passed a 200 ppb toluene vapor through the sample loop with 0.1 mL internal volume coupled to GC-FID and measured the area for a non-preconcentrated peak. Then we sampled the same toluene vapor at 40 mL/min for 35 min and injected it into a GC-FID to measure the area of the preconcentrated peak. The total volume of sample collection was 1.4 l. The chromatograms of the two sample injections overlap in Fig. 8. The insert shows a blow-up of the non-preconcentrated chromatogram. The sample mass collected from the μ-preconcentrator was 14,000 times larger than the injection from the 0.1 mL loop. The area ratio of the preconcentrated peak versus that of the original peak was 13,637. The difference between the actual value and the theoretical value was only −2.6%, which is within the variation range of 3.3% based on the reproducibility test from the last section.

3.6. Breakthrough behavior

Three VOCs with different volatilities: acetone, benzene and toluene, were used as representative compounds to test the sampling capacity of the μ-preconcentrator. A mixture consisting of 100 ppb of acetone, benzene and toluene was prepared in a Tedlar bag. The sampling flow rate was set at 40 mL/min. This was the maximum flow rate achievable due to the tradeoff between the suction force of the pump and the flow restriction of the μ-fluidic channel. It is generally known that a fast sampling flow will cause an early breakthrough due to the insufficiency in mass exchange of an adsorbent bed. This behavior can be predicted using Wheelers equation [8,9]. Therefore, we were testing the worst-case scenario in adsorption with this device. Any sampling flow rate that was lower than 40 mL/min can only show a better adsorption capacity than what was shown here. As shown in Fig. 9, both toluene and benzene showed no signs of a breakthrough up to 1.4 L of sample volume. The desorption peak area increased linearly as the sample volume increased. However, the desorption peak areas of acetone started to level off and deviated from the linear projection (dashed line) after 0.8 L of sample volume. These results indicate that the carbon film synthesized in the current study can provide sufficient sorption capacity for compounds with volatility lower than benzene. It might be insufficient for acetone if 1.0 L of sample volume is used as an arbitrary requirement for a maximum loading concentration of 100 ppb. This range of application is similar to that suggested for a Carbopack X, as cited in an earlier literature [6]. More

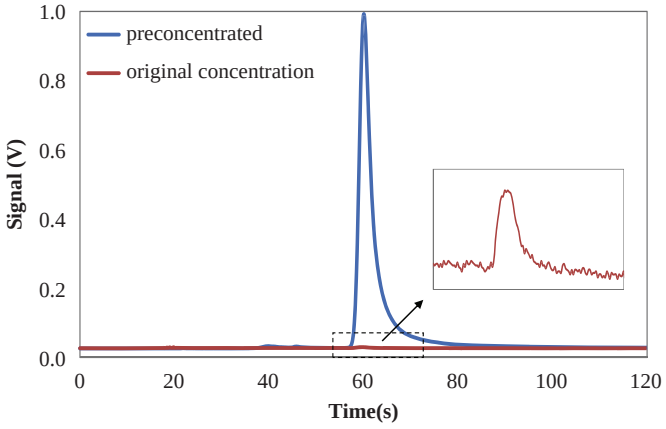

Fig. 8. Preconcentration factor test for toluene.

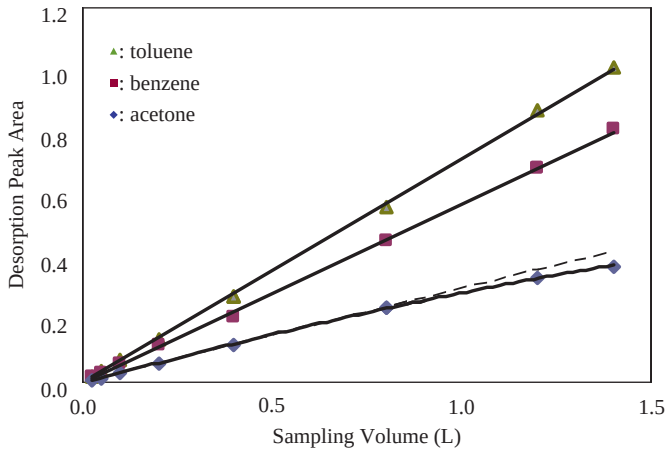

Fig. 9. Breakthrough curves of acetone, benzene and toluene (◆: acetone, ■: benzene, ▲:toluene).

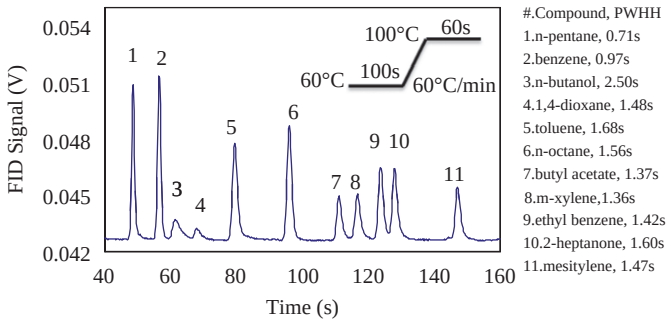

Fig. 10. Desorption chromatogram and peak width at half height for 11 selected VOCs.

preliminary capacity tests for 11 chemicals used in the flowing section and tests under high humidity are shown in the Appendix.

3.7. μ-Preconcentrator-GC-FID peak widths

Fig. 10 shows the chromatograms of the mixtures of 11 VOCs that were sampled and injected via the μ-preconcentrator. The concentration was 100 ppb for all 11 compounds and the sample volume was 50 mL. The compound names and peak widths at half height (PWHH) are listed on the legend of this figure. All PWHHs were less than 2 s, with the exception of n-butanol (2.5 s). The desorption flow rate was 3.0 mL/min which was the same as used in a previous non-MEMS preconcentrator study [5]. The PWHHs obtained in this study were narrower than non-MEMS preconcentrators, which were approximately 3 s. A previous study using a multistage adsorbent showed that compounds less volatile than m-xylene could result in a very broad injection band by thermal desorption from this adsorbent. It was the "on-column focusing" mechanism that reshaped the wide desorption bands into narrow peaks [6]. We believe the same was true for our μ-preconcentrator experiments. The inset in Fig. 10 shows the column temperature program that was used during desorption and chromatographic separation. The low volatile compounds could stack at the beginning section of the column and were gradually accelerated and eluted through the column as the GC temperature rose. The peak width of the lowest volatility compound, mesitylene, was even narrower than many high-volatile compounds. This was a clear indication of on-column focus.

3.8. General issues of design and performance

The SPME array design in the sampling chamber showed very good mass extraction efficiency. Both benzene and toluene were 100% trapped at a sampling flow rate of 40 mL/min. The gas–solid extraction efficiency might have been reduced if the sampling flow rates had been higher. However, 40 mL/min was the highest flow rate that was achievable due to the flow restriction of the current device. In order to reduce the flow restrictions of the fluidic channel, the diameter of μ-SPME needles must be smaller than the current design to leave a sufficient cross-section for gas flow. This was somehow limited by our capabilities of DRIE fabrication at this moment. Reducing sampling chamber length might be an alternative idea, but a reduction in total capacity might be a negative consequence.

The breakthrough of acetone was mainly due to the limited adsorption capacity of carbon film, not the insufficiency of the mass exchange between gas flow and solid adsorbent. If the gas–solid extraction were insufficient, all compounds would suffer from the same breakthrough result—not only high volatiles. The adsorbent that we developed in the present study is sufficient for benzene and compounds with lower volatility if the sampling requirement is 1.0 L for a maximum concentration of 100 ppb. Acetone or very volatile organic compounds (VVOCs), such as ethanol or methane, cannot be sufficiently trapped by cellulose-derived carbon film. We are still searching for a suitable precursor and the pyrolysis conditions to create a higher surface area carbon adsorbent for coating the μ-SPME array.

Prior to this study, most MEMS-based μ-preconcentrators that used a commercial carbon adsorbent faced the problem of trying to fill the μ-channel with fine carbon particles (i.e., 60/80 mesh or 80/100 mesh). Most of these carbon adsorbents are fragile and dusty, which is difficult to handle in clean-room processes. Although the thickness of adsorbent film in the present study was not uniform, it was very thin (i.e., all < 10 μm) by comparison with the granular diameter of all commercial adsorbents (typically > 100 μm), which ensured rapid thermal equilibrium and desorption. All μ-preconcentrator chips in the current design were anodic bonded and diced in a clean room before they were moved to chemical labs for precursor coating and carbonization. The packing process (e.g., wire bond, polyimide seal, etc.) can all be done outside of a clean room. The present study demonstrates a simple and robust way to grow adsorbent film inside a μ-preconcentrator chip after all clean-room processes have been completed.

4. Conclusion

We report the novel design, fabrication and evaluation of MEMS μ-preconcentrator for ambient VOCs sampling. Through the combination of a μ-SPME array structure and the direct synthesis of adsorbent film, the μ-preconcentrator presented in the current study showed sufficient gas–solid extraction efficiency. Due to the extreme thin adsorbent thickness inside the μ-preconcentrator, we believe that major restrictions for sampling flow arose from the MEMS structure of a μ-fluidic channel. Alternative designs to increase sampling flow and maintain mass exchange efficiency are underway. The breakthrough and desorption results in this research indicated that direct pyrolysis carbon film from cellulose can be used to replace some commercial granular adsorbents. Both the direct attachment of adsorbent film to the silicon structure and the thin film thicknesses allow rapid thermal equilibrium between the adsorbent and the heated structure of silicon. Our initial evaluations of performance have indicated that the capacity of this synthetic carbon film might not

yet be sufficient for trapping very high volatile compounds. The study to develop a higher-capacity adsorbent film for very high volatile compounds is also in progress.

Novelty statement

1. This is the first vapor preconcentrator employing both MEMS fabrication and direct pyrolysis carbon film on device.
2. The first design of micro-fabricated SPME array structure.

Acknowledgment

The National Science Council of ROC provided funding for this research under the following project number: 100-2113-M-003-001-MY2.

Appendix A. Supporting information

Supplementary data associated with this article can be found in the online version at http://dx.doi.org/10.1016/j.talanta.2012.09.031.

References

[1] E. Gallego, F.J. Roca, J.F. Perales, X. Guardino, Talanta 81 (2010) 916–924.
[2] F. Augusto, J. Koziel, J. Pawliszyn, Anal. Chem. 73 (2001) 481–486.
[3] Y. Gong, I.Y. Eom, D.W. Lou, D. Hein, J. Pawliszyn, Anal. Chem. 80 (2008) 7275–7282.
[4] B. Mendes, J. Goncalves, J.S. Camara, Talanta 88 (2012) 79–94.
[5] S.I. Ohira, K. Toda, Anal. Chim. Acta 619 (2008) 143–156.
[6] C. Feng, S. Mitra, J. Chromatogr. A 805 (1998) 169–176.
[7] C. Thammakhet, P. Thavarungkul, R. Brukh, S. Mitra, P. Kanatharana, J. Chromatogr. A 1072 (2005) 243–248.
[8] C.J. Lu, E.T. Zellers, Anal. Chem. 73 (2001) 3449–3457.
[9] C.J. Lu, E.T. Zellers, Analyst 127 (2002) 1061–1068.
[10] W.A. Groves, E.T. Zellers, G.C. Frye, Anal. Chim. Acta 371 (1998) 131–143.
[11] Q.Y. Cai, J. Park, D. Heldsinger, M.D. Hsiesh, E.T. Zellers, Sens. Actuators B: Chem. 62 (2000) 121–130.
[12] T.Y. Chen, M.J. Li, J.L. Wang, J. Chromatogr. A 976 (2002) 39–45.
[13] F. Blanco, X. Vilanova, V. Fierro, A. Celzard, P. Ivanov, E. Llobet, N. Canellas, J.L. Ramirez, X. Correig, Sens. Actuators B: Chem. 132 (2008) 90–98.
[14] H. Lahlou, X. Vilanova, V. Fierro, A. Celzard, E. Llobet, X. Correig, Sens. Actuators B: Chem. 154 (2011) 213–219.
[15] T. Nakamoto, Y. Isaka, T. Ishige, T. Moriizumi, Sens. Actuators B: Chem. 69 (2000) 90–98.
[16] P. Somboon, B. Wyszynski, T. Nakamoto, Sens. Actuators B: Chem. 127 (2007) 392–398.
[17] K. Cizek, C. Prior, C. Thammakhet, M. Galik, K. Linker, R. Tsui, A. Cagan, J. Wake, J. La Belle, J. Wang, Anal. Chim. Acta 661 (2010) 117–121.
[18] J. Ito, T. Nakamoto, H. Uematsu, Sens. Actuators B: Chem. 99 (2004) 431–436.
[19] C.E. Davis, C.K. Ho, R.C. Hughes, M.L. Thomas, Sens. Actuators B: Chem. 104 (2005) 207–216.
[20] C. Duran, X. Vilanova, J. Brezmes, E. Llobet, X. Correig, Sens. Actuators B: Chem. 131 (2008) 85–92.
[21] S.T. Hobson, S. Cemalovic, S.V. Patel, Analyst 137 (2012) 1284–1289.
[22] H. Lahlou, J.B. Sanchez, X. Vilanova, F. Berger, X. Correig, V. Fierro, A. Celzard, Sens. Actuators B: Chem. 156 (2011) 680–688.
[23] T. Sukaew, H. Chang, G. Serrano, E.T. Zellers, Analyst 136 (2011) 1664–1674.
[24] Q. Zhong, W.H. Steinecker, E.T. Zellers, Analyst 134 (2009) 283–293.
[25] C.J. Lu, J. Whiting, R.D. Sacks, E.T. Zellers, Anal. Chem. 75 (2003) 1400–1409.
[26] S.C. Terry, J.H. Jerman, J.B. Angell, IEEE Trans. Electron. Dev. 26 (1979) 1880.
[27] W. Kuipers, J. Muller, Talanta 82 (2010) 1674–1679.
[28] R.S. Jian, R.X. Huang, C.J. Lu, Talanta 88 (2012) 160–167.
[29] J.B. Sanchez, F. Berger, Talanta 80 (2009) 385–389.
[30] G.R. Lambertus, A. Elstro, K. Sensenig, J. Potkay, M. Agah, S. Scheuering, K. Wise, F. Dorman, R. Sacks, Anal. Chem. 76 (2004) 2629–2637.
[31] G.R. Lambertus, C.S. Fix, S.M. Reidy, R.A. Miller, D. Wheeler, E. Nazarov, R. Sacks, Anal. Chem. 77 (2005) 7563–7571.
[32] C.J. Lu, W.H. Steinecker, W.C. Tian, M.C. Oborny, J.M. Nichols, M. Agah, J.A. Potkay, H.K.L. Chan, J. Driscoll, R.D. Sacks, K.D. Wise, S.W. Pang, E.T. Zellers, Lab Chip 5 (2005) 1123–1131.
[33] I. Voiculescu, M. Zaghloul, N. Narasimhan, Trends Anal. Chem. 27 (2008) 327–345.
[34] E.H.M. Camara, P. Breuil, D. Briand, L. Guillot, C. Pijolat, N.F. de Rooij, Sens. Actuators B: Chem. 148 (2010) 610–619.
[35] I. Gracia, P. Ivanov, F. Blanco, N. Sabate, X. Vilanova, X. Correig, L. Fonseca, E. Figueras, J. Santander, C. Cane, Sens. Actuators B: Chem. 135 (2008) 52–56.
[36] A.M. Ruiz, I. Gracia, N. Sabate, P. Ivanov, A. Sanchez, M. Duch, M. Gerboles, A. Moreno, C. Cane, Sens. Actuators A: Phys. 135 (2007) 192–196.
[37] W.C. Tian, S.W. Pang, C.J. Lu, E.T. Zellers, J. Microelectromech. Syst. 12 (2003) 264–272.
[38] W.C. Tian, H.K.L. Chan, C.J. Lu, S.W. Pang, E.T. Zellers, J. Microelectromech. Syst. 14 (2005) 498–507.
[39] P. Ivanov, F. Blanco, I. Gracia, N. Sabate, A.M. Ruiz, X. Vilanova, X. Correig, L. Fonseca, E. Figueras, J. Santander, C. Cane, Sens. Actuators B: Chem. 127 (2007) 288–294.
[40] I. Gracia, P. Ivanov, F. Blanco, N. Sabate, X. Vilanova, X. Correig, L. Fonseca, E. Figueras, J. Santander, C. Cane, Sens. Actuators B: Chem. 132 (2008) 149–154.
[41] A.B. Alamin Dow, W. Lang, Sens. Actuators B: Chem. 151 (2010) 304–307.
[42] A.B. Alamin Dow, A. Sklorz, W. Lang, Sens. Actuators A: Phys. 167 (2011) 226–230.
[43] C. Pijolat, M. Camara, J. Courbat, J.-P. Viricelle, D. Briand, N.F. de Rooij, Sens. Actuators B: Chem. 127 (2007) 179–185.
[44] E.H.M. Camara, P. Breuil, D. Briand, N.F. de Rooij, C. Pijolat, Anal. Chim. Acta 688 (2011) 175–182.
[45] M. Martin, M. Crain, K. Walsh, R.A. McGill, E. Houser, J. Stepnowski, S. Stepnowski, H.D. Wu, S. Ross, Sens. Actuators B: Chem. 126 (2007) 447–454.
[46] B. Alfeeli, D. Cho, M. Ashraf-Khorassani, L.T. Taylor, M. Agah, Sens. Actuators B: Chem. 133 (2008) 24–32.
[47] B. Alfeeli, L.T. Taylor, M. Agah, Microchem. J. 95 (2010) 259–267.
[48] B. Alfeeli, V. Jain, R.K. Johnson, F.L. Beyer, J.R. Heflin, M. Agah, Microchem. J. 95 (2010) 259–267.
[49] M. Valcarcel, S. Cardenas, B.M. Simonet, Y. Moliner-Martinez, R. Lucena, Trends Anal. Chem. 27 (2008) 34–43.